

Non-stationary Spatial Modelling with Applications to Spatial Prediction of Precipitation

Geir-Arne Fuglstad^{*1}, Daniel Simpson¹, Finn Lindgren², and Håvard Rue¹

¹Department of Mathematical Sciences, NTNU, Norway

²Department of Mathematical Sciences, University of Bath, UK

June 3, 2013

Abstract

A non-stationary spatial Gaussian random field (GRF) is described as the solution of an inhomogeneous stochastic partial differential equation (SPDE), where the covariance structure of the GRF is controlled by the coefficients in the SPDE. This allows for a flexible way to vary the covariance structure, where intuition about the resulting structure can be gained from the local behaviour of the differential equation. Additionally, computations can be done with computationally convenient Gaussian Markov random fields which approximate the true GRFs. The model is applied to a dataset of annual precipitation in the conterminous US. The non-stationary model performs better than a stationary model measured with both CRPS and the logarithmic scoring rule.

Keywords: Bayesian, Non-stationary, Spatial modelling, Stochastic partial differential equation, Gaussian random field, Gaussian Markov random field, Annual precipitation

1 Introduction

Classical geostatistical models are usually based on stationary Gaussian random fields (GRFs) with covariates that capture important structure in the mean. However, for environmental phenomena there is often no reason to believe that the covariance structures of the processes are stationary. For example, the spatial distribution of precipitation is greatly affected by topography. Some of the effects can be captured in the mean, but other effects such as decreased dependence between two locations because there is a mountain between them is something which should enter in the covariance structure. The main focus of this paper is on allowing a flexible model for the covariance structure of the process. The goal is to improve spatial predictions at unmeasured locations.

The dataset used consists of monthly precipitation measured in millimetres per month for the conterminous US for the years 1895–1997 and is available at the web page <http://www.image.ucar.edu/GSP/Data/US.monthly.met/>. There are a total of 11918 measurement stations, but measurements are only available for some stations each month and the rest of the stations have infill values (Johns et al., 2003). The monthly data for 1981 is aggregated to yearly precipitation for those stations which have measurements available for all months. This leaves a total of 7040

^{*}fuglstad@math.ntnu.no

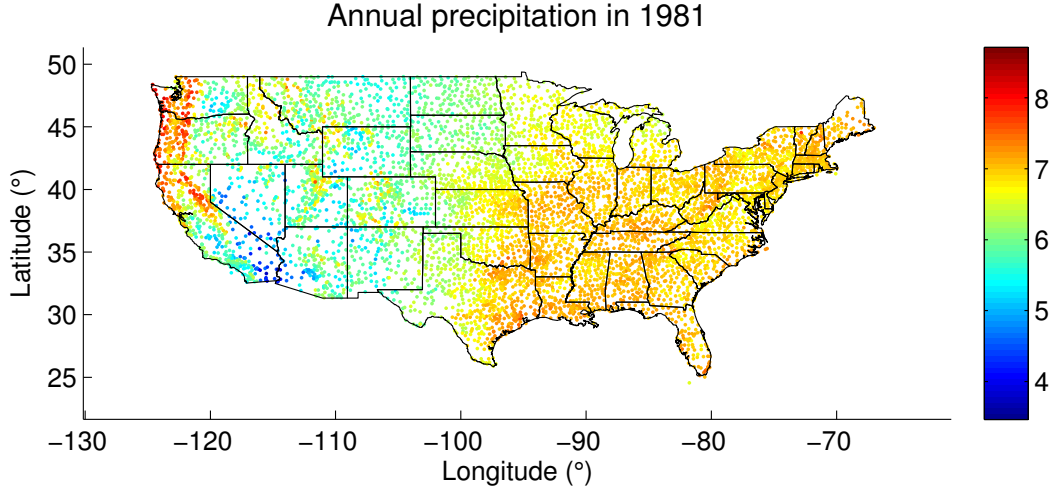


Figure 1: The logarithm of total yearly precipitation measured in millimetres at 7040 locations in the conterminous US for the year 1981.

measurements of yearly precipitation in 1981. After aggregating the data, the logarithm of each value is taken. This gives the observations shown in Figure 1. The only covariate available in the dataset is the elevation at each station, and since the focus of the paper is on the covariance structure, no work was done to find new covariates from other sources. Paciorek and Schervish (2006) previously used the same dataset to study a kernel-based non-stationary model for annual precipitation, but their work was restricted to the state of Colorado.

The traditional approaches to spatial modelling are based on covariance functions and are severely limited by a cubic increase in computation time as a function of the number of observations and prediction locations. In this paper we take a different approach based on the connection between stochastic partial differential equations (SPDEs) and some classes of GRFs that was developed by Lindgren et al. (2011). The main computational benefit of this approach comes from a transition from a covariance function based representation to a Gaussian Markov random field (GMRF) (Rue and Held, 2005) based formulation. In a similar way as a spatial GMRF describes local behaviour for a discretely indexed process, an SPDE describes local behaviour for a continuously indexed process. This continuous description of local behaviour can be transferred to a GMRF approximation of the solution of the SPDE and gives a GMRF with a spatial Markovian structure that can be exploited in computations.

Lindgren et al. (2011) showed that Matérn-like GRFs can be constructed from a relatively simple stationary SPDE, which can be thought of as a continuous linear filter driven by Gaussian white noise. From this starting point it is possible to make a spatially varying linear filter that imposes different smoothing of the Gaussian white noise at different locations. This leads to a non-stationary GRF whose global covariance structure is modelled through the local behaviour at each location. Such SPDE-based non-stationary GRFs have previously been applied to global ozone data (Bolin and Lindgren, 2011) and annual precipitation data for Norway (Ingebrigtsen et al., 2013). Their models preserved the computational benefits of GMRFs, but allowed for non-stationary covariance structures. The model used in this paper is constructed in a similar fashion, but with a focus on varying the local anisotropy as in Fuglstad et al. (2013).

The closest among the more well-known methods for non-stationary spatial modelling is the

deformation method (Sampson and Guttorp, 1992), where an isotropic process is made non-stationary by deforming the base space. However, in the method presented in this paper it is not the deformation itself that is modelled, but rather the distance measure in the space. Loosely speaking, one controls local range and anisotropy. This usually leads to distance measures that cannot be described by a deformation of \mathbb{R}^2 and require embeddings into higher dimensional spaces. But all deformations can be described by a change of the distance measure. The original formulation of the deformation method has later been extended to Bayesian variants (Damian et al., 2001; 2003; Schmidt and O’Hagan, 2003; Schmidt et al., 2011).

Another type of methods with some connection to the SPDE-based models is the kernel methods (Higdon, 1998; Paciorek and Schervish, 2006) in which a spatially varying kernel is convolved with Gaussian white noise. The solutions of the SPDE can be formulated in the same manner, but this is not practical and would lead to something more directly connected to the covariance matrix as opposed to the conditional formulation where the precision matrix is directly available. The already mentioned methods are the most closely relevant ones, but there is a large literature on other non-stationary methods (Haas, 1990; 1990b; Kim et al., 2005; Fuentes, 2001; 2002; 2002b).

The paper is divided into five sections. Section 2 describes the theoretical basis for the spatial model. The connection between the coefficients that control the SPDE and the resulting GRF is discussed, and a way to parametrize the GRF is presented. In Section 3, a Bayesian hierarchical model using the GRF is constructed and the resulting posterior distribution is explicitly given. Then in Section 4 the hierarchical model is applied to annual precipitation in the conterminous US for 1981. The predictions of the non-stationary model is compared to the stationary model. Lastly, the paper ends with discussion and concluding remarks in Section 5.

2 The spatial model

2.1 The SPDE-based model

A good spatial model should provide a useful way to model spatial phenomena. For a non-stationary model, it is not easy to create a global covariance function when one only has intuition about local behaviour. Consider the situation in Figure 2. The left hand side and right hand side has locally large “range” in the horizontal direction and somewhat shorter “range” in the vertical direction, and the middle area has locally much shorter “range” in the horizontal direction, but slightly longer in the vertical direction. From the figure one can see that for the point in the middle, the chosen contours look more or less unaffected by the two other regions since they are fully contained in the middle region, but that for the point on the left hand side and the point on the right hand side, there is much skewness introduced by the transition into a different region.

It would be very hard to directly construct a fitting correlation function for this situation. Therefore, this example provides a strong case for the use of SPDE-based models. This is exactly the type of behaviour they can describe. With the SPDE-based approach one does not try to model the global behaviour directly, but rather how the “range” behaves locally. This implies that specifying a specific correlation between two locations is hard, but this is besides the point. The correlation should be determined by what happens between the locations. That is whether there are plains or lakes where one might believe that the correlation decreases slowly or a mountain where one might believe that the correlation decreases quickly. A great thing about this type of local specification is that it naturally leads to a spatial GMRF that has good computational properties. Since each location is conditionally dependent only on locations close to itself, the precision matrix is sparse.

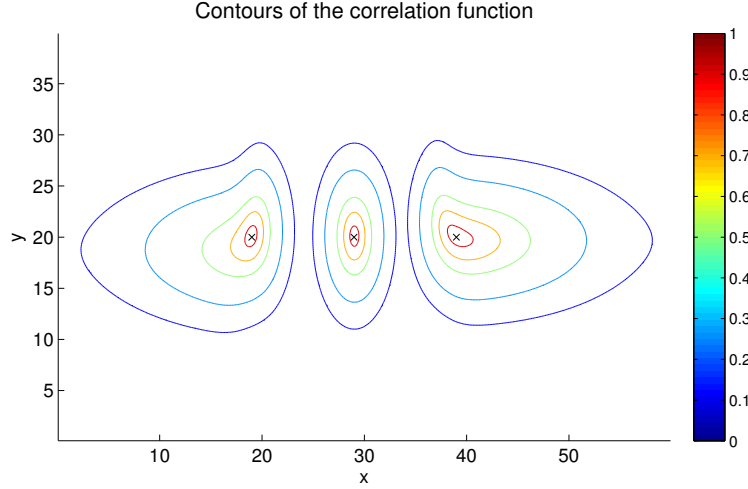


Figure 2: Example of a correlation function caused by varying local behaviour. For each location marked with a black cross, the 0.9, 0.7, 0.5, 0.25 and 0.12 level contours of the correlation function are shown.

The starting point for the non-stationary SPDE-based model is the stationary SPDE introduced in Lindgren et al. (2011),

$$(\kappa^2 - \nabla \cdot \nabla)u(\mathbf{s}) = \sigma \mathcal{W}(\mathbf{s}), \quad \mathbf{s} \in \mathbb{R}^2, \quad (1)$$

where $\kappa > 0$ and $\sigma > 0$ are constants, $\nabla = (\frac{\partial}{\partial x}, \frac{\partial}{\partial y})^T$ and \mathcal{W} is standard Gaussian white noise. This SPDE basically describes the GRF u as a smoothed version of the Gaussian white noise on the right hand side. Whittle (1954) showed that any stationary solution of this SPDE has the Matérn covariance function

$$r(\mathbf{s}_1, \mathbf{s}_2) = \frac{\sigma^2}{4\pi\kappa^2} (\kappa \|\mathbf{s}_2 - \mathbf{s}_1\|) K_1(\kappa \|\mathbf{s}_2 - \mathbf{s}_1\|), \quad (2)$$

where K_1 is the modified Bessel function of second kind, order 1. This covariance function is a member of one of the more commonly used families of covariance functions, and one can see from Equation (2) that one can first use κ to select the range and then σ to achieve the desired marginal variance.

The next step is to generate a GRF with an anisotropic Matérn covariance function. The reason behind the isotropy in the SPDE above is that the Laplacian, $\Delta = \nabla \cdot \nabla$ is invariant to a change of coordinates that only involves rotation and translation. To change this a 2×2 matrix $\mathbf{H} > 0$ is introduced into the operator to give the SPDE

$$(\kappa^2 - \nabla \cdot \mathbf{H} \nabla)u(\mathbf{s}) = \sigma \mathcal{W}(\mathbf{s}). \quad (3)$$

This choice is closely related to a change of coordinates $\tilde{\mathbf{s}} = \mathbf{H}^{1/2} \mathbf{s}$ and gives the covariance function

$$r(\mathbf{s}_1, \mathbf{s}_2) = \frac{\sigma^2}{4\pi\kappa^2 \sqrt{\det(\mathbf{H})}} (\kappa \|\mathbf{H}^{-1/2}(\mathbf{s}_2 - \mathbf{s}_1)\|) K_1(\kappa \|\mathbf{H}^{-1/2}(\mathbf{s}_2 - \mathbf{s}_1)\|). \quad (4)$$

Compared to Equation (2) there is a change in the marginal variance and a directionality is introduced through a distance measure that is different than the standard Euclidean distance.

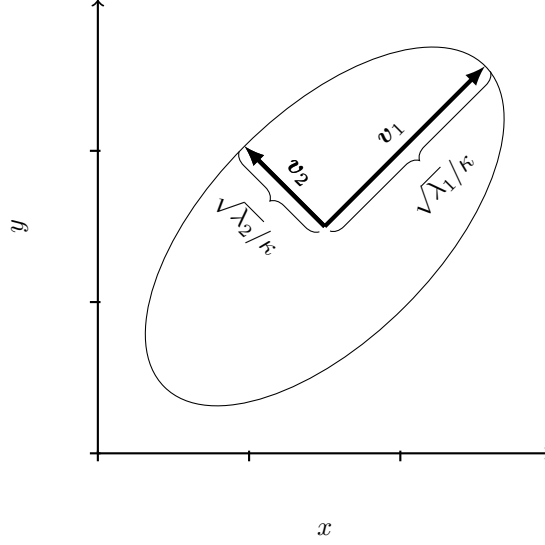


Figure 3: Isocorrelation curve for the 0.6 level, where $(\lambda_1, \mathbf{v}_1)$ and $(\lambda_2, \mathbf{v}_2)$ are the eigenpairs of \mathbf{H} .

Figure 3 shows how the eigenpairs of \mathbf{H} and the value of κ act together to control range. One can see that this leads to elliptic isocovariance curves. In what follows σ is assumed to be equal to 1 since the marginal variance can be controlled by varying κ^2 and \mathbf{H} together.

The final step is to construct a non-stationary GRF where the local behaviour at each location is governed by SPDE (3), but $\sigma = 1$ and the values of κ^2 and \mathbf{H} vary over the domain. The intention is to create a GRF by chaining together processes with different covariance structures. The SPDE becomes

$$(\kappa^2(\mathbf{s}) - \nabla \cdot \mathbf{H}(\mathbf{s}) \nabla) u(\mathbf{s}) = \mathcal{W}(\mathbf{s}). \quad (5)$$

For technical reasons concerned with the discretization in the next section, κ^2 is required to be continuous and \mathbf{H} is required to be continuously differentiable. See Fuglstad et al. (2013) for a study of the case where κ^2 is constant and \mathbf{H} varies.

2.2 Gaussian Markov random field approximation

SPDE (5) describes the covariance structure of a GRF, but the information must be brought into a form which is useful for computations. The first thing to notice is that the operator in front of u only contains multiplications with functions and first order and second order derivatives. All of these operations involve only the local properties of u at each location. This means that if u is discretized, the corresponding discretized operators (matrices) should only involve variables close to each other. This leads to a sparse GMRF which possesses approximately the same covariance structure as u .

The first step in creating the GMRF is to restrict SPDE (5) to a bounded domain,

$$(\kappa^2(\mathbf{s}) - \nabla \cdot \mathbf{H}(\mathbf{s}) \nabla) u(\mathbf{s}) = \mathcal{W}(\mathbf{s}), \quad \mathbf{s} \in \mathcal{D} = [A_1, B_1] \times [A_2, B_2] \subset \mathbb{R}^2,$$

where $B_1 > A_1$ and $B_2 > A_2$. This restriction necessitates a boundary condition to make the distribution useful and proper. For technical reasons the boundary condition chosen is zero flux across the boundaries. The derivation of a discretized version of this SPDE on a grid is somewhat

involved, but for periodic boundary conditions the derivation can be found in Fuglstad et al. (2013). The boundary conditions in this problem involve a slight change in that derivation.

For a regular $m \times n$ grid of \mathcal{D} , the end result is the matrix equation

$$\mathbf{A}(\kappa^2, \mathbf{H})\mathbf{u} = \frac{1}{\sqrt{V}}\mathbf{z},$$

where V is the area of each cell in the grid, \mathbf{u} corresponds to the values of u on the cells in the regular grid stacked column-wise, $\mathbf{z} \sim \mathcal{N}_{mn}(\mathbf{0}, \mathbf{I}_{mn})$ and $\mathbf{A}(\kappa^2, \mathbf{H})$ is a discretized version of $(\kappa^2 - \nabla \cdot \mathbf{H} \nabla)$. This matrix equation leads to the distribution

$$\mathbf{u} \sim \mathcal{N}_{mn}(\mathbf{0}, \mathbf{Q}(\kappa^2, \mathbf{H})^{-1}), \quad (6)$$

where $\mathbf{Q}(\kappa^2, \mathbf{H}) = \mathbf{A}(\kappa^2, \mathbf{H})^T \mathbf{A}(\kappa^2, \mathbf{H}) V$. The precision matrix has up to 25 non-zero elements in each row, corresponding to the point itself, its eight closest neighbours and the eight closest neighbours of the eight closest neighbours.

This type of construction alleviates one of the largest problems with GMRFs, namely that they are hard to specify. The computational benefits of spatial GMRFs are well known, but a GMRF needs to be constructed through its conditional distributions. This is notoriously hard to do for non-stationary models. But with the type of derivation outlined above it is possible to model the problem with an SPDE and then automatically find a GMRF corresponding to this model, but with the computational benefits of GMRFs preserved.

2.3 Decomposition of \mathbf{H}

The function \mathbf{H} must give positive definite 2×2 matrices at each location. One usual way to do this is to use two strictly positive functions λ_1 and λ_2 for the eigenvalues and a function ϕ for the angle between the x -axis and the eigenvector associated with λ_1 . However, with a slight re-parametrization \mathbf{H} can be written as the sum of an isotropic effect, described by a constant times the identity matrix, plus an additional anisotropic effect, described by direction and magnitude. Write \mathbf{H} as a function of the scalar functions γ , v_x and v_y by

$$\mathbf{H}(\mathbf{s}) = \gamma(\mathbf{s})\mathbf{I}_2 + \begin{bmatrix} v_x(\mathbf{s}) \\ v_y(\mathbf{s}) \end{bmatrix} \begin{bmatrix} v_x(\mathbf{s}) & v_y(\mathbf{s}) \end{bmatrix},$$

where γ is required to be strictly positive. The eigendecomposition of this matrix has eigenvalue $\lambda_1(\mathbf{s}) = \gamma(\mathbf{s})$ with eigenvector $\mathbf{v}_1(\mathbf{s}) = (v_x(\mathbf{s}), v_y(\mathbf{s}))$ and eigenvalue $\lambda_2(\mathbf{s}) = \gamma(\mathbf{s}) + v_x(\mathbf{s})^2 + v_y(\mathbf{s})^2$ with eigenvector $\mathbf{v}_2(\mathbf{s}) = (-v_y(\mathbf{s}), v_x(\mathbf{s}))$. From Figure 3 this means that for a stationary model, γ affects the length of the shortest semi-axis of the isocorrelation curves and \mathbf{v} specifies the direction of and how much larger the longest semi-axis is.

2.4 Parametrization of the model

Since the focus lies on allowing flexible covariance structures, some representation of the functions κ^2 , γ , v_x and v_y is needed. To ensure positivity of κ^2 and γ , they are first transformed into $\log(\kappa^2)$ and $\log(\gamma)$. The choice was made to make $\log(\kappa^2)$, $\log(\gamma)$, v_x and v_y Gaussian processes a priori. This requires both a finite dimensional representation of each function and appropriate priors to connect the parameters in each function to each other. The steps that follow are the same for each function. Therefore, they are only shown for $\log(\kappa^2)$.

A priori $\log(\kappa^2)$ is given the distribution generated from the SPDE

$$-\Delta \log(\kappa^2(\mathbf{s})) = \mathcal{W}_\kappa(\mathbf{s}) / \sqrt{\tau_\kappa}, \quad \mathbf{s} \in \mathcal{D}, \quad (7)$$

where $\tau_\kappa > 0$ is a scale hyperparameter, with an additional requirement of zero derivatives at the edges. This extra requirement is used to restrict the resulting distribution so it is only invariant to the addition of a constant function, and the hyperparameter is used to regulate how much $\log(\kappa^2)$ can vary from a constant function. The prior defined through SPDE (7) is in this paper called a two-dimensional second-order random walk due to its similarity to a one-dimensional second-order random walk (Lindgren and Rue, 2008).

The next step is to expand $\log(\kappa^2)$ in a basis through a linear combination of basis functions,

$$\log(\kappa^2(\mathbf{s})) = \sum_{i=1}^k \sum_{j=1}^l \alpha_{ij} f_{ij}(\mathbf{s}),$$

where $\{\alpha_{ij}\}$ are the parameters and $\{f_{ij}\}$ are real-valued basis functions. For convenience, the basis is chosen in such a way that all basis functions satisfy the boundary conditions specified in SPDE (7). If this is done, one does not have to think more about the boundary condition. The remaining tasks are then to decide which basis functions to use and what distribution the parameters should be given.

Due to a desire to make \mathbf{H} continuously differentiable and a desire to have “local” basis functions, the basis functions are chosen to be based on 2-dimensional, second-order B-splines (piecewise-quadratic functions). The basis is constructed as a tensor product of two 1-dimensional B-spline bases constrained to satisfy the boundary condition.

The final step is to determine a Gaussian distribution for the parameters such that the distribution of $\log(\kappa^2)$ is close to a solution of SPDE (7). The approach taken is based on a least-squares formulation of the solution and is described in Appendix A. Let $\boldsymbol{\alpha}$ be the $\{\alpha_{ij}\}$ parameters stacked row-wise, then the result is that $\boldsymbol{\alpha}$ should be given a zero-mean Gaussian distribution with precision matrix $\tau_\kappa \mathbf{Q}_{\text{RW2}}$. This matrix has rank $(kl - 1)$ and the distribution is invariant to the addition of a vector of only the same values, but for convenience the distribution will still be written as $\boldsymbol{\alpha} \sim \mathcal{N}_{kl}(\mathbf{0}, \mathbf{Q}_{\text{RW2}}^{-1}/\tau_\kappa)$.

3 Hierarchical model

3.1 Full model

Observations y_1, y_2, \dots, y_N are made at locations $\mathbf{s}_1, \mathbf{s}_2, \dots, \mathbf{s}_N$. The observed value at each location is assumed to be the sum of a fixed effect due to covariates, a spatial “smooth” effect and a random effect. The covariates at location \mathbf{s}_i is described by the p -dimensional row vector $\mathbf{x}(\mathbf{s}_i)^T$ and the spatial field is denoted by u . This gives the equation

$$y_i = \mathbf{x}(\mathbf{s}_i)^T \boldsymbol{\beta} + u(\mathbf{s}_i) + \epsilon_i,$$

where $\boldsymbol{\beta}$ is a p -variate random vector for the coefficients of the covariates and $\epsilon_i \sim \mathcal{N}(0, 1/\tau_{\text{noise}})$ is the random effect for observation i .

The u is modelled as in Section 2 and a GMRF approximation is introduced for computations. In this GMRF approximation the domain is divided into a regular grid consisting of rectangular cells and each element of the GMRF approximation describes the average value on one of these cells. So $u(\mathbf{s}_i)$ is replaced with the approximation $\mathbf{e}(\mathbf{s}_i)^T \mathbf{u}$, where $\mathbf{e}(\mathbf{s}_i)^T$ is the mn -dimensional row vector selecting the element of \mathbf{u} which corresponds to the cell which contains location \mathbf{s}_i . In total, this gives

$$\mathbf{y} = \mathbf{X}\boldsymbol{\beta} + \mathbf{E}\mathbf{u} + \boldsymbol{\epsilon}, \tag{8}$$

where $\mathbf{y} = (y_1, y_2, \dots, y_N)$, the matrix \mathbf{X} has $\mathbf{x}(\mathbf{s}_1)^T, \dots, \mathbf{x}(\mathbf{s}_N)^T$ as rows and the matrix \mathbf{E} has $\mathbf{e}(\mathbf{s}_1)^T, \dots, \mathbf{e}(\mathbf{s}_N)^T$ as rows. The model for the observations can also be written in the form

$$\mathbf{y}|\boldsymbol{\beta}, \mathbf{u}, \log(\tau_{\text{noise}}) \sim \mathcal{N}_N(\mathbf{X}\boldsymbol{\beta} + \mathbf{E}\mathbf{u}, \mathbf{I}_N/\tau_{\text{noise}}).$$

The parameter τ_{noise} acts as the precision of a joint effect from measurement noise and small scale spatial variation (Diggle et al., 2007).

This can be turned into a full Bayesian model by providing priors for the two remaining parameters. The p -dimensional random variable $\boldsymbol{\beta}$ is given a weak Gaussian prior,

$$\boldsymbol{\beta} \sim \mathcal{N}_p(\mathbf{0}, \mathbf{I}_p/\tau_{\beta}),$$

and the precision parameter τ_{noise} is given an improper, uniform prior on log-scale,

$$\log(\tau_{\text{noise}}) \sim \mathcal{U}(0, \infty).$$

To describe the full hierarchical model it is necessary to introduce some symbols to denote the parameters and hyperparameters in the spatial field \mathbf{u} . Denote the parameters that control $\log(\kappa^2)$, $\log(\gamma)$, v_x and v_y by $\boldsymbol{\alpha}_1$, $\boldsymbol{\alpha}_2$, $\boldsymbol{\alpha}_3$ and $\boldsymbol{\alpha}_4$, respectively. Further, denote the corresponding scale hyperparameters that controls the degree of smoothing for each function by τ_1 , τ_2 , τ_3 and τ_4 . With this notation the full model becomes

$$\text{Stage 1: } \mathbf{y}|\boldsymbol{\beta}, \mathbf{u}, \log(\tau_{\text{noise}}) \sim \mathcal{N}_N(\mathbf{X}\boldsymbol{\beta} + \mathbf{E}\mathbf{u}, \mathbf{I}_N/\tau_{\text{noise}})$$

$$\text{Stage 2: } \mathbf{u}|\boldsymbol{\alpha}_1, \boldsymbol{\alpha}_2, \boldsymbol{\alpha}_3, \boldsymbol{\alpha}_4 \sim \mathcal{N}_{nm}(\mathbf{0}, \mathbf{Q}^{-1}), \quad \boldsymbol{\beta} \sim \mathcal{N}_p(\mathbf{0}, \mathbf{I}_p/\tau_{\beta})$$

$$\text{Stage 3: } \log(\tau_{\text{noise}}) \sim \mathcal{U}(0, \infty), \quad \boldsymbol{\alpha}_i|\tau_i \sim \mathcal{N}_{kl}(\mathbf{0}, \mathbf{Q}_{\text{RW2}}^{-1}/\tau_i) \text{ for } i = 1, 2, 3, 4,$$

where τ_1 , τ_2 , τ_3 , τ_4 and τ_{β} are hyperparameters that must be pre-selected in some way.

3.2 Posterior distribution and inference

Denote the covariance parameters by $\boldsymbol{\theta} = (\boldsymbol{\alpha}_1, \boldsymbol{\alpha}_2, \boldsymbol{\alpha}_3, \boldsymbol{\alpha}_4, \log(\tau_{\text{noise}}))$, then the posterior distribution of interest is $\pi(\boldsymbol{\theta}|\mathbf{y})$. The derivation of this distribution involves integrating out Stage 2 of the hierarchical model. It is possible to do this explicitly (up to a constant) due to the fact that all distributions are Gaussian given the covariance parameters.

First, treat the fixed effect and the spatial effect together with $\mathbf{z} = (\mathbf{u}^T, \boldsymbol{\beta}^T)$. This leads to

$$\mathbf{z}|\boldsymbol{\theta} \sim \mathcal{N}_{mn+p}(\mathbf{0}, \mathbf{Q}_z^{-1})$$

and

$$\mathbf{y}|\mathbf{z}, \boldsymbol{\theta} \sim \mathcal{N}_N(\mathbf{S}\mathbf{z}, \mathbf{I}_N/\tau_{\text{noise}}),$$

where

$$\mathbf{S} = [\mathbf{E} \quad \mathbf{X}]$$

and

$$\mathbf{Q}_z = \begin{bmatrix} \mathbf{Q} & \mathbf{0} \\ \mathbf{0} & \tau_{\beta}\mathbf{I}_p \end{bmatrix}.$$

Then apply the Bayesian formula to integrate out \mathbf{z} from the joint distribution of \mathbf{y} , \mathbf{z} and $\boldsymbol{\theta}$ as shown in Appendix B. This gives the full log-posterior

$$\begin{aligned} \log(\pi(\boldsymbol{\theta}|\mathbf{y})) = & \text{Const} - \frac{1}{2} \sum_{i=1}^4 \boldsymbol{\alpha}_i^T \mathbf{Q}_{\text{RW2}} \boldsymbol{\alpha}_i \cdot \tau_i + \frac{1}{2} \log(\det(\mathbf{Q}_z)) + \frac{N}{2} \log(\tau_{\text{noise}}) + \\ & - \frac{1}{2} \log(\det(\mathbf{Q}_C)) - \frac{1}{2} \boldsymbol{\mu}_C^T \mathbf{Q}_z \boldsymbol{\mu}_C - \frac{\tau_{\text{noise}}}{2} (\mathbf{y} - \mathbf{S}\boldsymbol{\mu}_C)^T (\mathbf{y} - \mathbf{S}\boldsymbol{\mu}_C), \end{aligned} \quad (9)$$

where $\mathbf{Q}_C = \mathbf{Q}_z + \mathbf{S}^T \mathbf{S} \cdot \tau_{\text{noise}}$ and $\boldsymbol{\mu}_C = \mathbf{Q}_C^{-1} \mathbf{S}^T \mathbf{y} \cdot \tau_{\text{noise}}$.

The properties of $\boldsymbol{\theta}|\mathbf{y}$ are not easily available from Equation (9). As such, the inference and the prediction are done in something close to an empirical Bayes setting. The parameters are first estimated by the maximum a posteriori (MAP) estimator, $\hat{\boldsymbol{\theta}}$, and then the values at new locations \mathbf{y}^* are predicted with $\mathbf{y}^*|\hat{\boldsymbol{\theta}}, \mathbf{y}$. However, the hyperparameters that control the priors for the covariance parameters are very hard to estimate. There is not enough information to estimate the hyperparameters in the third stage of the hierarchical model. Thus they are selected with a cross-validation procedure based on a score for the predictions.

During implementation it became apparent that an analytic expression for the gradient was needed for the optimization to converge. Its form is given in Appendix C, and its value can be computed for less cost than a finite difference approximation of the gradient with the number of parameters used in the application in this paper. The calculations require the use of techniques for calculating only parts of the inverse of a sparse precision matrix (Gelfand et al., 2010, Sections 12.1.7.10–12.1.7.12).

4 Application

In this section the models and the estimation procedures presented in Sections 2 and 3 are applied to annual precipitation data for the conterminous US. A stationary and a non-stationary model is fitted to the data and the quality of the predictions are compared.

4.1 The dataset

The dataset is described in the introduction and consists of log-transformed values of the annual precipitation measured in millimetres in 1981 for the conterminous US for 7040 measurement stations. The values are shown in Figure 1. The elevation of each station is available and is used together with a joint mean for the fixed effect. This means that the design matrix, \mathbf{X} , in Equation (8) contains two columns. The first column contains only ones, and corresponds to the joint mean, and the second column contains elevations measured in kilometres. The coefficients of the fixed effect, $\boldsymbol{\beta}$, is given the vague prior $\boldsymbol{\beta} \sim \mathcal{N}_2(\mathbf{0}, \mathbf{I}_2 \cdot 10^4)$.

4.2 Stationary model

The spatial effect is constructed on a rectangular domain with longitudes from 130.15°W to 60.85°W and latitudes from 21.65°N to 51.35°N. This is larger than the actual size of the conterminous US as can be seen in Figure 1. This is done to reduce boundary effects. The domain is discretized into a 400 × 200 grid and the parameters $\log(\kappa^2)$, $\log(\gamma)$, v_x , v_y and $\log(\tau_{\text{noise}})$ are estimated. In this case the second order random walk prior is not used as no basis (except a constant) is needed for the functions. Each parameter is given a uniform prior and the parameters are estimated with MAP estimates. The estimated values with associated approximate standard deviations are shown in Table 1. The approximate standard deviations are calculated from the observed information matrix.

From Section 2.1 one can see that the estimated model implies a covariance function approximately equal to the Matérn covariance function

$$r(\mathbf{s}_1, \mathbf{s}_2) = \hat{\sigma}^2 \left\| \left(\hat{\mathbf{H}}/\hat{\kappa}^2 \right)^{-1/2} (\mathbf{s}_2 - \mathbf{s}_1) \right\| K_1 \left(\left\| \left(\hat{\mathbf{H}}/\hat{\kappa}^2 \right)^{-1/2} (\mathbf{s}_2 - \mathbf{s}_1) \right\| \right),$$

Table 1: Estimated values of the parameters and associated approximate standard deviations for the stationary model.

Parameter	Estimate	Standard deviation
$\log(\kappa^2)$	-1.75	0.15
$\log(\gamma)$	-0.272	0.042
v_x	0.477	0.053
v_y	-0.313	0.057
$\log(\tau_{\text{noise}})$	4.266	0.030

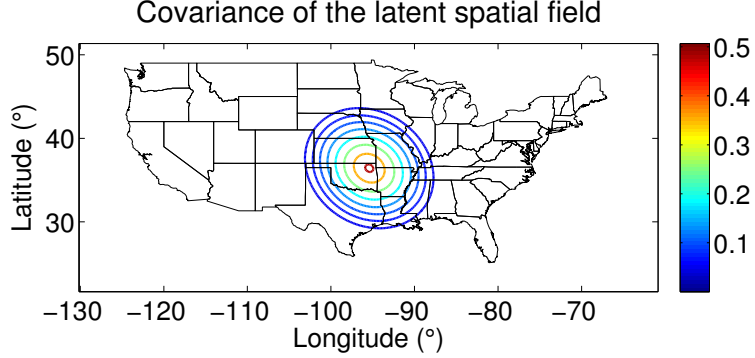


Figure 4: The 0.95, 0.70, 0.50, 0.36, 0.26, 0.19, 0.14 and 0.1 level correlation contours of the estimated covariance function for the stationary model.

where $\hat{\sigma}^2 = 0.505$ and

$$\frac{\hat{\mathbf{H}}}{\hat{\kappa}^2} = \begin{bmatrix} 5.71 & -0.86 \\ -0.86 & 4.96 \end{bmatrix},$$

with an additional nugget effect with precision $\hat{\tau}_{\text{noise}} = 71.2$. Figure 4 shows contours of the estimated covariance function with respect to one location. One can see that the model gives high dependence within a typical-sized state, whereas there is little dependence between the centres of different typically-sized states.

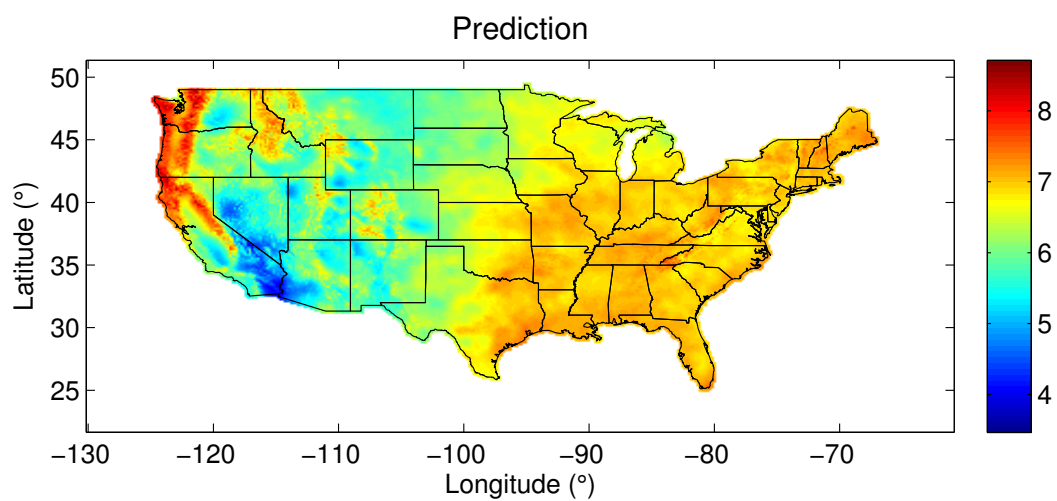
Next, the parameter values are used together with the observed logarithms of annual precipitations to predict the logarithm of annual precipitation at the centre of each cell in the discretization. This gives 400×200 locations to predict. The elevation covariate for each location is selected from bilinear interpolation from the closest points in the high resolution elevation data set GLOBE (Hastings et al., 1999). The predictions and prediction standard deviations are shown in Figure 5. Since the observations are contained within the conterminous US, the locations outside are coloured white.

4.3 Non-stationary model

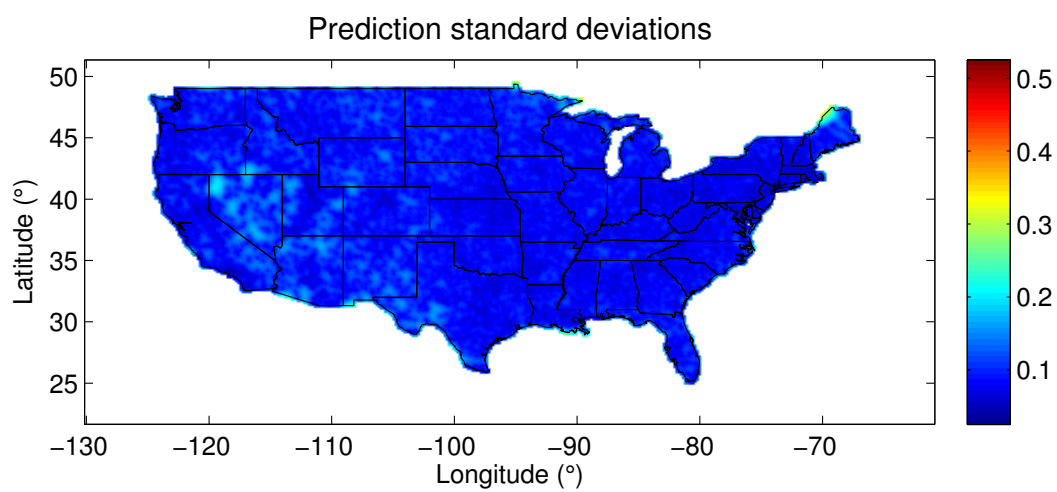
This section uses the same domain size and observations as in Section 4.2.

4.3.1 Selection of the smoothing parameters

As discussed in Section 3.1, the hyperparameters τ_1 , τ_2 , τ_3 and τ_4 , that appear in the priors for the functions $\log(\kappa^2)$, $\log(\gamma)$, v_x and v_y , must be pre-selected in some way before the rest



(a) Prediction



(b) Prediction standard deviations

Figure 5: Predicted values and prediction standard deviations for the stationary model.

of the inference is done. Since these hyperparameters control smoothing in the third stage of a hierarchical spatial model, there is little information available about them in the data. Attempts were made to give them Gamma priors and infer them together with $\alpha_1, \alpha_2, \alpha_3, \alpha_4$ and $\log(\tau_{\text{noise}})$ as MAP estimates, but this leads to estimates that are too influenced by the Gamma priors.

The hyperparameters are chosen with 5-fold cross-validation based on the log-predictive density. The data is randomly divided into five parts and in turn one part is used as test data and the other four parts are used as training data. For each choice of τ_1, τ_2, τ_3 and τ_4 the cross-validation error is calculated by

$$\text{CV}(\tau_1, \tau_2, \tau_3, \tau_4) = -\frac{1}{5} \sum_{i=1}^5 \log(\pi(\mathbf{y}_i^* | \mathbf{y}_i, \hat{\boldsymbol{\theta}}_i)),$$

where \mathbf{y}_i^* is the test data and $\hat{\boldsymbol{\theta}}_i$ is the MAP estimate of the parameters based on the training data \mathbf{y}_i using the selected τ -values. This function is calculated for $\log(\tau_i) \in \{2, 4, 6, 8\}$ for $i = 1, 2, 3, 4$. The model is run on a 200×100 grid with 8×4 basis functions for each function. The choice that gave the smallest cross-validation error was $\log(\tau_1) = 2$, $\log(\tau_2) = 4$, $\log(\tau_3) = 2$ and $\log(\tau_4) = 8$.

4.3.2 Parameter estimates

The non-stationary spatial model is constructed with the same discretization of the domain as the stationary model. But in the non-stationary spatial model each of the four functions in the SPDE is given a 16×8 basis with a second-order random walk prior. The hyperparameters in the priors are set to the values from Section 4.3.1. Together with the precision parameter of the random effect this gives a total of 513 parameters. These parameters are estimated together with a MAP estimate. It is worth noting that there are not 513 “free” parameters as most of them are connected together in four different Gaussian process priors. This means that an increase in the number of parameters would mean increases in the resolutions of these Gaussian processes.

The nugget effect has an estimated precision of $\hat{\tau}_{\text{noise}} = 107.4$, and the estimates of κ^2 and \mathbf{H} are not shown since the exact values themselves are not interesting. However, from the estimated functions it is possible to approximately visualize the resulting covariance structure of the latent field. This can be done with the covariance function in Equation (4) which describes the covariances of a stationary model. For each location in the grid the marginal standard deviation is calculated using the Matérn covariance function with the parameters at that location. This gives the results shown in Figure 6(a). Then for selected locations the correlation function defined by the parameters at those locations are used to draw 0.7 level correlation contours as shown in Figure 6(b).

The figures based on stationary models give a quick indication of the structure, but are only approximations. The exact marginal standard deviations and 0.7 level correlation contours for the same locations as above are given in Figure 6(c) and Figure 6(d). From these figures one can see that there is good correspondence between the approximations and the exact calculations. It is interesting to observe that the exact correlation contours have the same general shape, but are stretched corresponding to whether the range of the stationary models are increasing or decreasing. The exact contours for the locations around longitude 100° are “larger” in the east direction and “smaller” in the west direction than the contours based on the stationary approximation.

It is worth mentioning that since only one realization is used, one cannot expect the estimated covariance structure to be “the true” covariance structure. It is impossible to separate the effects due to non-stationarity in the mean and the effects due to non-stationarity in the covariance

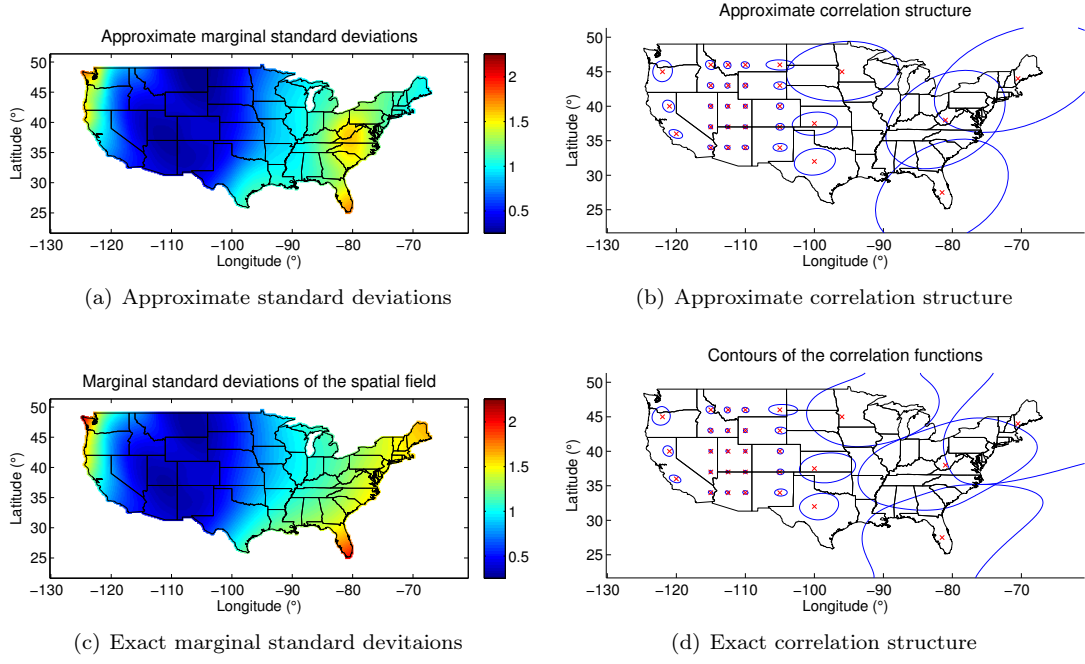


Figure 6: Estimated covariance structure of the spatial field. (a) Marginal standard deviations of the stationary models defined by the parameter values in each point (b) Contours of 0.7 correlation for the stationary models defined by the parameter values at selected locations marked with red crosses (c) Exact marginal standard deviations (d) Exact contours of 0.7 correlation for selected locations marked with red crosses

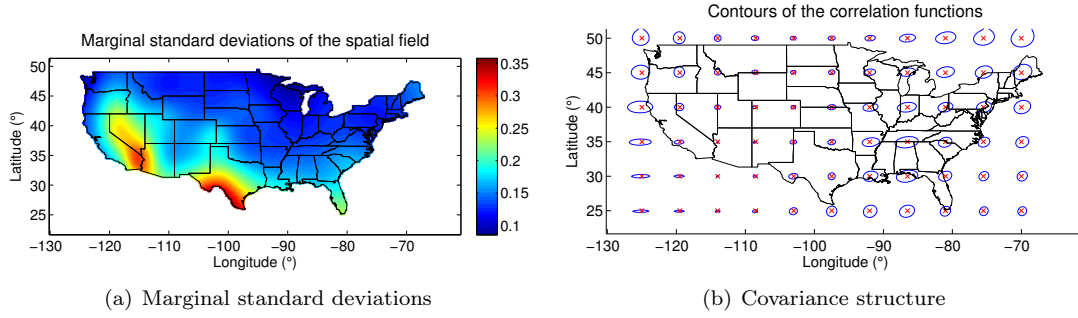


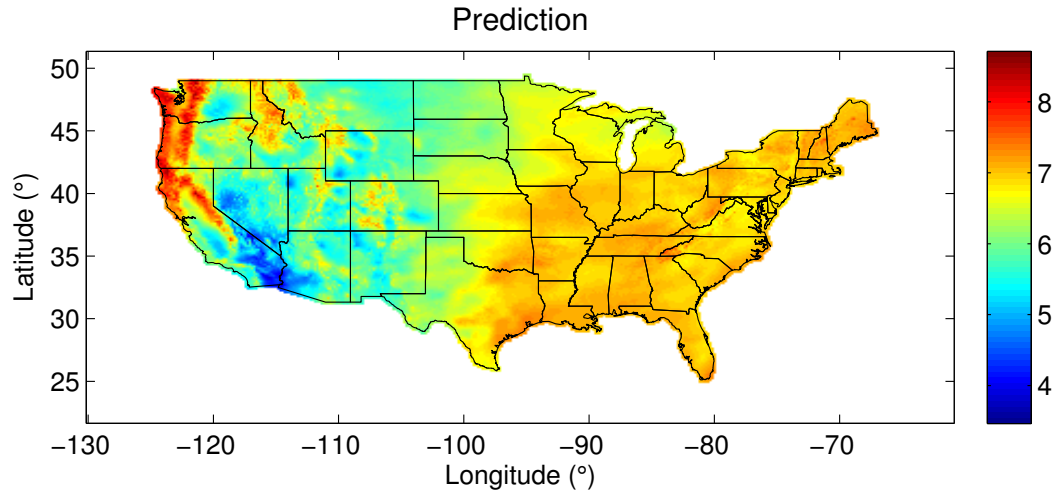
Figure 7: Estimate of the prior covariance structure with an extra covariate. (a) Marginal standard deviations (b) Contours of 0.7 level correlation for selected locations marked with red crosses

structure. Therefore, the estimated structure must be understood to say something about both how well the covariates describe the data at different locations and the non-stationarity in the covariance structure. In this case there is a good fit for the elevation covariate in the mountainous areas in the western part, but it offers less information in the eastern part. From Figure 1 one can see that at around longitude 97° W there is an increase in precipitation which cannot be explained by elevation, and thus not captured by the covariates. In the areas with long correlation “range”, the spatial field is “approaching” a second-order random walk.

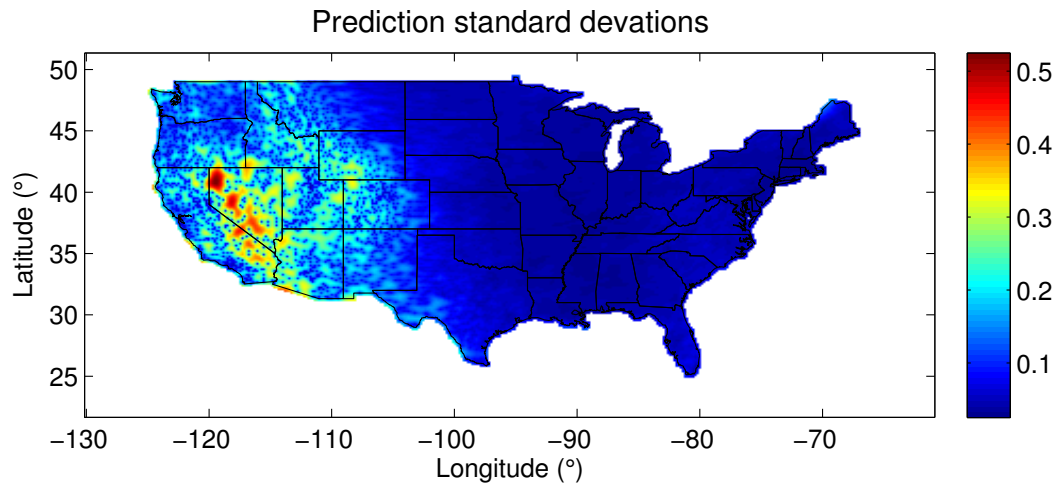
In the dataset used for this application there is more information available about the covariance structure than has been used. In addition to 1981 there is precipitation data available for 102 other years. These data could be used to create a full spatio-temporal model, but this is not the intention of this paper. Instead the effect of the additional information will be illustrated by extracting a covariate which explains much of the non-stationarity in the mean. For each location used in the 1981 dataset take the mean over the 102 other years (using the fill-in values as necessary). This covariate used together with a joint mean gives the marginal standard deviations and correlation contours shown in Figure 7. One can see that the amount of non-stationarity captured by the mean has a large impact on the resulting covariance structure, and one should strive to include the information that is available. But one can see from the Figure 7 that there is still evidence of non-stationarity in the covariance structure with this additional covariate.

4.3.3 Prediction

In the same way as in Section 4.2 the logarithm of annual precipitation is predicted at the centre of each cell in the discretization. This gives predictions for 400×200 regularly distributed locations, where the value of the elevation covariate at each location is selected with bilinear interpolation from the closest points in the GLOBE (Hastings et al., 1999) dataset. The prediction and prediction standard deviations are shown in Figure 8. In the same way as for the stationary model, the values outside the conterminous US are coloured white. One can see that the overall look of the predictions is similar to the predictions from the stationary model, but that the prediction standard deviations differ. In the non-stationary model it varies how quickly the prediction standard deviations increase as one moves away from an observed location.



(a) Prediction



(b) Prediction standard deviations

Figure 8: Predictions and prediction standard deviations for the non-stationary model for the logarithm of annual precipitation in the conterminous US in 1981 measured in millimetres.

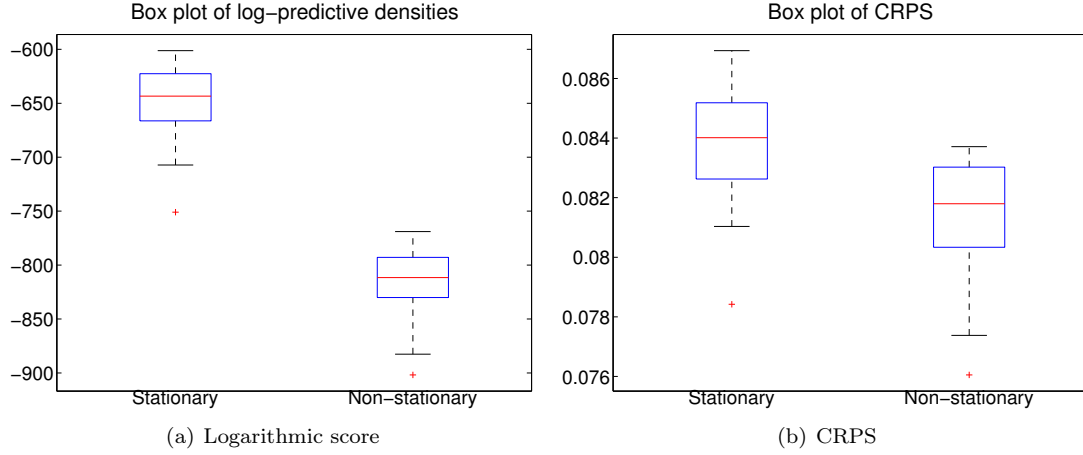


Figure 9: Box-plot of prediction scores from the stationary and the non-stationary model. 20% of the locations are randomly chosen to be held out and the remaining 80% are used to estimate parameters and predict the 20% held out data. This was repeated 20 times. Lower is better.

4.4 Comparison of the stationary and the non-stationary model

The predictions of the stationary model and the non-stationary model are compared with the continuous rank probability score (CRPS) (Gneiting et al., 2005) and the logarithmic scoring rule. CRPS is defined for a univariate distribution as

$$\text{crps}(F, y) = \int_{-\infty}^{\infty} (F(y) - \mathbb{1}(y \leq t))^2 dt,$$

where F is the distribution function of interest, y is an observation and $\mathbb{1}$ is the indicator function. This gives a measure of how well a single observation fits a distribution. The total score is calculated as the average CRPS for the test data,

$$\text{CRPS} = \frac{1}{N} \sum_{i=1}^N \text{crps}(F_k, y_k),$$

where $\{y_k\}$ is the test data and $\{F_k\}$ are the corresponding marginal prediction distributions given the estimated covariance parameters and the training data. The logarithmic scoring rule is based on the joint distribution of the test data \mathbf{y}^* given the estimated covariance parameters $\hat{\boldsymbol{\theta}}$ and the training data \mathbf{y} ,

$$\text{LogScore} = -\log \pi(\mathbf{y}^* | \hat{\boldsymbol{\theta}}, \mathbf{y}).$$

The comparison is done with holdout sets. For each holdout set 20% of the locations are chosen randomly. The remaining 80% of the locations are used to estimate the parameters and to predict the values at the locations in the holdout set. This procedure is repeated 20 times. For each repetition both the CRPS and the logarithmic score is calculated. From Figure 9 one can see that measured by both scores the non-stationary model gives better predictions.

5 Discussion and conclusion

SPDE-based modelling offers a different point of view than modelling based on covariance functions. The focus is shifted from global properties to local properties. The object which is modelled is the “local” dependences around a point, which are then automatically combined into a global structure. This offers some benefits in the sense that it is easier to have intuition about local behaviour, but on the other hand the SPDE introduces coefficients whose influence on the global structure might not be immediately obvious. But it is possible to gain intuition about the global behaviour through the stationary models defined by the parameters at each point.

In this paper it has been demonstrated that a non-stationary spatial model can be constructed from an SPDE in such a way that the resulting model can be estimated and used for prediction. The modelling can be done with an SPDE while the computations are done with a GMRF approximation. This makes the estimation computationally feasible for the number of observations used in the application to annual precipitation. The model allows a flexible structure which gives completely different covariance structures in the western and eastern part of the conterminous US. Additionally, the non-stationary model leads to better prediction than the stationary model measured both with CRPS and the logarithmic scoring rule.

The estimated covariance structure in itself is not that interesting since it is a combination of unexplained non-stationarity in the mean and actual non-stationarity in the covariance structure. Non-stationarity from these two sources are indistinguishable with a single realization. If one includes a covariate in the mean that better explains the non-stationarity, one ends up with a very different covariance structure. However, such extra information is not available in the spatial smoothing type application treated here.

The major challenge remaining is selecting the smoothing hyperparameters used in the priors for the coefficients of the SPDE. These control smoothing at the third stage of a hierarchical spatial model and are not easily inferred. Using cross-validation to select them is both an inefficient solution and an unsatisfactory solution from a Bayesian point of view. The major problem is the number of parameters in the model, which makes it hard to study the marginal posterior distribution of the smoothing parameters. It might be of interest to look into simulation based methods.

A Derivation of the second-order random walk prior

Each function, f , is a priori modelled as a Gaussian process described by the SPDE

$$-\Delta f(\mathbf{s}) = \frac{1}{\sqrt{\tau}} \mathcal{W}(\mathbf{s}), \quad \mathbf{s} \in \mathcal{D} = [A_1, B_1] \times [A_2, B_2], \quad (\text{A.1})$$

where $A_1 < B_1$, $A_2 < B_2$ and $\tau > 0$, \mathcal{W} is standard Gaussian white noise and $\Delta = \frac{\partial^2}{\partial x^2} + \frac{\partial^2}{\partial y^2}$, with the Neumann boundary condition of zero normal derivatives at the edges. In practice this is approximated by representing f as a linear combination of basis elements $\{f_{ij}\}$ weighted by Gaussian distributed weights $\{\alpha_{ij}\}$,

$$f(\mathbf{s}) = \sum_{i=1}^K \sum_{j=1}^L \alpha_{ij} f_{ij}(\mathbf{s}).$$

The basis functions are constructed from separate bases $\{g_i\}$ and $\{h_j\}$ for the x -coordinate and the y -coordinate, respectively,

$$f_{ij}(\mathbf{s}) = g_i(x)h_j(y). \quad (\text{A.2})$$

For convenience each basis function is assumed to fulfil the boundary condition of zero normal derivative at the edges.

Let $\boldsymbol{\alpha} = \text{vec}([\alpha_{ij}]_{ij})$, then the task is to find the best Gaussian distribution for $\boldsymbol{\alpha}$. Where “best” is used in the sense of making the resulting distribution for f “close” to a solution of SPDE (A.1). This is done by a least-squares approach where the vector created from doing inner products of the left hand side with $-\Delta f_{kl}$ must be equal in distribution to the vector created from doing the same to the right hand side,

$$\text{vec}([\langle -\Delta f, -\Delta f_{kl} \rangle_{\mathcal{D}}]_{kl}) \stackrel{d}{=} \text{vec}([\langle \mathcal{W}, -\Delta f_{kl} \rangle_{\mathcal{D}}]_{kl}). \quad (\text{A.3})$$

First, calculate the inner product that is needed

$$\begin{aligned} \langle -\Delta g_i h_j, -\Delta g_k h_l \rangle_{\mathcal{D}} &= \langle \Delta g_i h_j, \Delta g_k h_l \rangle_{\mathcal{D}} \\ &= \left\langle \left(\frac{\partial^2}{\partial x^2} g_i \right) h_j + g_i \frac{\partial^2}{\partial y^2} h_j, \left(\frac{\partial^2}{\partial x^2} g_k \right) h_l + g_k \frac{\partial^2}{\partial y^2} h_l \right\rangle_{\mathcal{D}}. \end{aligned}$$

The bilinearity of the inner product can be used to expand the expression in a sum of four innerproducts. Each of these inner products can then be written as a product of two inner products. Due to lack of space this is not done explicitly, but one of these terms is, for example,

$$\left\langle \left(\frac{\partial^2}{\partial x^2} g_i \right) h_j, \left(\frac{\partial^2}{\partial x^2} g_k \right) h_l \right\rangle_{\mathcal{D}} = \left\langle \frac{\partial^2}{\partial x^2} g_i, \frac{\partial^2}{\partial y^2} g_k \right\rangle_{[A_1, B_1]} \langle h_j, h_l \rangle_{[A_2, B_2]}.$$

By inserting Equation (A.2) into Equation (A.3) and using the above derivations together with integration by parts one can see that the left hand side becomes

$$\text{vec}([\langle -\Delta f, -\Delta f_{kl} \rangle_{\mathcal{D}}]_{kl}) = \mathbf{C} \boldsymbol{\alpha},$$

where $\mathbf{C} = \mathbf{G}_2 \otimes \mathbf{H}_0 + 2\mathbf{G}_1 \otimes \mathbf{H}_1 + \mathbf{G}_0 \otimes \mathbf{H}_2$ with

$$\mathbf{G}_n = \left[\left\langle \frac{\partial^n}{\partial x^n} g_i, \frac{\partial^n}{\partial x^n} g_j \right\rangle_{[A_1, B_1]} \right]_{i,j}$$

and

$$\mathbf{H}_n = \left[\left\langle \frac{\partial^n}{\partial y^n} h_i, \frac{\partial^n}{\partial y^n} h_j \right\rangle_{[A_2, B_2]} \right]_{i,j}.$$

The right hand side is a Gaussian random vector where the covariance between the position corresponding to α_{ij} and the position corresponding to α_{kl} is given by

$$\langle -\Delta f_{ij}, -\Delta f_{kl} \rangle_{\mathcal{D}}.$$

Thus the covariance matrix of the right hand side must be \mathbf{C} and Equation (A.3) can be written in matrix form as

$$\mathbf{C}\boldsymbol{\alpha} = \mathbf{C}^{1/2}\mathbf{z},$$

where $\mathbf{z} \sim \mathcal{N}_{KL}(\mathbf{0}, \mathbf{I}_{KL})$. This means that $\boldsymbol{\alpha}$ should be given the precision matrix $\mathbf{Q} = \mathbf{C}$. Note that \mathbf{C} might be singular due to invariance to some linear combination of the basis elements.

B Conditional distributions

From the hierarchical model

$$\text{Stage 1: } \mathbf{y}|\mathbf{z}, \boldsymbol{\theta} \sim \mathcal{N}_N(\mathbf{S}\mathbf{z}, \mathbf{I}_N/\tau_{\text{noise}})$$

$$\text{Stage 2: } \mathbf{z}|\boldsymbol{\theta} \sim \mathcal{N}_{mn+p}(\mathbf{0}, \mathbf{Q}_z^{-1}),$$

the posterior distribution $\pi(\boldsymbol{\theta}|\mathbf{y})$ can be derived explicitly. There are three steps involved.

B.1 Step 1

Calculate the distribution $\pi(\mathbf{z}|\boldsymbol{\theta}, \mathbf{y})$ up to a constant,

$$\begin{aligned} \pi(\mathbf{z}|\boldsymbol{\theta}, \mathbf{y}) &\propto \pi(\mathbf{z}, \boldsymbol{\theta}, \mathbf{y}) \\ &= \pi(\boldsymbol{\theta})\pi(\mathbf{z}|\boldsymbol{\theta})\pi(\mathbf{y}|\boldsymbol{\theta}, \mathbf{z}) \\ &\propto \exp\left(-\frac{1}{2}(\mathbf{z} - \mathbf{0})^T \mathbf{Q}_z (\mathbf{z} - \mathbf{0}) - \frac{1}{2}(\mathbf{y} - \mathbf{S}\mathbf{z})^T \mathbf{I}_N \cdot \tau_{\text{noise}} (\mathbf{y} - \mathbf{S}\mathbf{z})\right) \\ &\propto \exp\left(-\frac{1}{2}(\mathbf{z}^T (\mathbf{Q}_z + \tau_{\text{noise}} \mathbf{S}^T \mathbf{S}) \mathbf{z} - 2\mathbf{z}^T \mathbf{S}^T \mathbf{y} \cdot \tau_{\text{noise}})\right) \\ &\propto \exp\left(-\frac{1}{2}(\mathbf{z} - \boldsymbol{\mu}_C)^T \mathbf{Q}_C (\mathbf{z} - \boldsymbol{\mu}_C)\right), \end{aligned}$$

where $\mathbf{Q}_C = \mathbf{Q}_z + \mathbf{S}^T \mathbf{S} \cdot \tau_{\text{noise}}$ and $\boldsymbol{\mu}_C = \mathbf{Q}_C^{-1} \mathbf{S}^T \mathbf{y} \cdot \tau_{\text{noise}}$. This is recognized as a Gaussian distribution

$$\mathbf{z}|\boldsymbol{\theta}, \mathbf{y} \sim \mathcal{N}_N(\boldsymbol{\mu}_C, \mathbf{Q}_C^{-1}).$$

B.2 Step 2

Integrate out \mathbf{z} from the joint distribution of \mathbf{z} , $\boldsymbol{\theta}$ and \mathbf{y} via the Bayesian rule,

$$\begin{aligned} \pi(\boldsymbol{\theta}, \mathbf{y}) &= \frac{\pi(\boldsymbol{\theta}, \mathbf{z}, \mathbf{y})}{\pi(\mathbf{z}|\boldsymbol{\theta}, \mathbf{y})} \\ &= \frac{\pi(\boldsymbol{\theta})\pi(\mathbf{z}|\boldsymbol{\theta})\pi(\mathbf{y}|\mathbf{z}, \boldsymbol{\theta})}{\pi(\mathbf{z}|\boldsymbol{\theta}, \mathbf{y})}. \end{aligned}$$

The left hand side of the expression does not depend on the value of \mathbf{z} , therefore the right hand side may be evaluated at any desired value of \mathbf{z} . Evaluating at $\mathbf{z} = \boldsymbol{\mu}_C$ gives

$$\begin{aligned}\pi(\boldsymbol{\theta}, \mathbf{y}) &\propto \frac{\pi(\boldsymbol{\theta})\pi(\mathbf{z} = \boldsymbol{\mu}_C)\pi(\mathbf{y}|\mathbf{z} = \boldsymbol{\mu}_C, \boldsymbol{\theta})}{\pi(\mathbf{z} = \boldsymbol{\mu}_C|\boldsymbol{\theta}, \mathbf{y})} \\ &\propto \pi(\boldsymbol{\theta}) \frac{|\mathbf{Q}_z|^{1/2} |\mathbf{I}_N \cdot \tau_{\text{noise}}|^{1/2}}{|\mathbf{Q}_C|^{1/2}} \exp\left(-\frac{1}{2} \boldsymbol{\mu}_C^T \mathbf{Q}_z \boldsymbol{\mu}_C\right) \times \\ &\times \exp\left(-\frac{1}{2} (\mathbf{y} - \mathbf{S} \boldsymbol{\mu}_C)^T \mathbf{I}_N \cdot \tau_{\text{noise}} (\mathbf{y} - \mathbf{S} \boldsymbol{\mu}_C)\right) \times \\ &\times \exp\left(+\frac{1}{2} (\boldsymbol{\mu}_C - \boldsymbol{\mu}_C)^T \mathbf{Q}_C (\boldsymbol{\mu}_C - \boldsymbol{\mu}_C)\right).\end{aligned}$$

B.3 Step 3

Condition on \mathbf{y} to get the desired conditional distribution,

$$\begin{aligned}\log(\pi(\boldsymbol{\theta}|\mathbf{y})) &= \text{Const} + \log(\pi(\boldsymbol{\theta})) + \frac{1}{2} \log(\det(\mathbf{Q}_z)) + \frac{N}{2} \log(\tau_{\text{noise}}) + \\ &- \frac{1}{2} \log(\det(\mathbf{Q}_C)) - \frac{1}{2} \boldsymbol{\mu}_C^T \mathbf{Q}_z \boldsymbol{\mu}_z - \frac{\tau_{\text{noise}}}{2} (\mathbf{y} - \mathbf{S} \boldsymbol{\mu}_C)^T (\mathbf{y} - \mathbf{S} \boldsymbol{\mu}_C).\end{aligned}\quad (\text{B.1})$$

C Analytic expression for the gradient

This appendix shows the derivation of the derivative of the log-likelihood. Choose the evaluation point $\mathbf{z} = \mathbf{0}$ in Appendix B.2 to find

$$\begin{aligned}\log(\pi(\boldsymbol{\theta}, \tau_{\text{noise}}|\mathbf{y})) &= \text{Const} + \log(\pi(\boldsymbol{\theta}, \tau_{\text{noise}})) + \frac{1}{2} \log(\det(\mathbf{Q}_z)) + \frac{N}{2} \log(\tau_{\text{noise}}) + \\ &- \frac{1}{2} \log(\det(\mathbf{Q}_C)) - \frac{\tau_{\text{noise}}}{2} \mathbf{y}^T \mathbf{y} + \frac{1}{2} \boldsymbol{\mu}_C^T \mathbf{Q}_C \boldsymbol{\mu}_C.\end{aligned}$$

This is just a rewritten form of Equation (B.1) which is more convenient for the calculation of the gradient, and which separates the τ_{noise} parameter from the rest of the covariance parameters. First some preliminary results are presented, then the derivatives are calculated with respect to θ_i and lastly the derivatives are calculated with respect to $\log(\tau_{\text{noise}})$.

Begin with simple preliminary formulas for the derivatives of the conditional precision matrix with respect to each of the parameters,

$$\frac{\partial}{\partial \theta_i} \mathbf{Q}_C = \frac{\partial}{\partial \theta_i} (\mathbf{Q} + \mathbf{S}^T \mathbf{S} \cdot \tau_{\text{noise}}) = \frac{\partial}{\partial \theta_i} \mathbf{Q} \quad (\text{C.1})$$

and

$$\frac{\partial}{\partial \log(\tau_{\text{noise}})} \mathbf{Q}_C = \frac{\partial}{\partial \log(\tau_{\text{noise}})} (\mathbf{Q} + \mathbf{S}^T \mathbf{S} \cdot \tau_{\text{noise}}) = \mathbf{S}^T \mathbf{S} \cdot \tau_{\text{noise}}. \quad (\text{C.2})$$

C.1 Derivative with respect to θ_i

First the derivatives of the log-determinants can be handled by an explicit formula (Petersen and Pedersen, 2012)

$$\begin{aligned}\frac{\partial}{\partial \theta_i}(\log(\det(\mathbf{Q})) - \log(\det(\mathbf{Q}_C))) &= \text{Tr}(\mathbf{Q}^{-1} \frac{\partial}{\partial \theta_i} \mathbf{Q}) - \text{Tr}(\mathbf{Q}_C^{-1} \frac{\partial}{\partial \theta_i} \mathbf{Q}_C) \\ &= \text{Tr} \left[(\mathbf{Q}^{-1} - \mathbf{Q}_C^{-1}) \frac{\partial}{\partial \theta_i} \mathbf{Q} \right].\end{aligned}$$

Then the derivative of the quadratic forms are calculated

$$\begin{aligned}\frac{\partial}{\partial \theta_i} \left(-\frac{1}{2} \mathbf{y}^T \mathbf{y} \cdot \tau_{\text{noise}} + \frac{1}{2} \boldsymbol{\mu}_C^T \mathbf{Q}_C \boldsymbol{\mu}_C \right) &= 0 + \frac{\partial}{\partial \theta_i} \left(\frac{1}{2} \mathbf{y}^T \tau_{\text{noise}} \mathbf{S} \mathbf{Q}_C^{-1} \mathbf{S}^T \tau_{\text{noise}} \mathbf{y} \right) \\ &= -\frac{1}{2} \mathbf{y}^T \tau_{\text{noise}} \mathbf{S} \mathbf{Q}_C^{-1} \left(\frac{\partial}{\partial \theta_i} \mathbf{Q}_C \right) \mathbf{Q}_C^{-1} \mathbf{S}^T \tau_{\text{noise}} \mathbf{y} \\ &= -\frac{1}{2} \boldsymbol{\mu}_C^T \left(\frac{\partial}{\partial \theta_i} \mathbf{Q} \right) \boldsymbol{\mu}_C.\end{aligned}$$

Combining these gives

$$\frac{\partial}{\partial \theta_i} \log(\pi(\boldsymbol{\theta}, \tau_{\text{noise}} | \mathbf{y})) = \frac{\partial}{\partial \theta_i} \log(\pi(\boldsymbol{\theta}, \tau_{\text{noise}})) + \frac{1}{2} \text{Tr} \left[(\mathbf{Q}^{-1} - \mathbf{Q}_C^{-1}) \frac{\partial}{\partial \theta_i} \mathbf{Q} \right] - \frac{1}{2} \boldsymbol{\mu}_C^T \left(\frac{\partial}{\partial \theta_i} \mathbf{Q} \right) \boldsymbol{\mu}_C$$

C.2 Derivative with respect to $\log(\tau_{\text{noise}})$

First calculate the derivative of the log-determinants

$$\begin{aligned}\frac{\partial}{\partial \log(\tau_{\text{noise}})} (N \log(\tau_{\text{noise}}) - \log(\det(\mathbf{Q}_C))) &= N - \text{Tr} \left(\mathbf{Q}_C^{-1} \frac{\partial}{\partial \log(\tau_{\text{noise}})} \mathbf{Q}_C \right) \\ &= N - \text{Tr} (\mathbf{Q}_C^{-1} \mathbf{S}^T \mathbf{S} \cdot \tau_{\text{noise}}).\end{aligned}$$

Then the derivative of the quadratic forms

$$\begin{aligned}\frac{\partial \left(-\frac{1}{2} \mathbf{y}^T \mathbf{y} \cdot \tau_{\text{noise}} + \frac{1}{2} \boldsymbol{\mu}_C^T \mathbf{Q}_C \boldsymbol{\mu}_C \right)}{\partial \log(\tau_{\text{noise}})} &= -\frac{1}{2} \mathbf{y}^T \mathbf{y} \cdot \tau_{\text{noise}} + \frac{\partial}{\partial \log(\tau_{\text{noise}})} \frac{1}{2} \mathbf{y}^T \tau_{\text{noise}} \mathbf{S} \mathbf{Q}_C^{-1} \mathbf{S}^T \tau_{\text{noise}} \mathbf{y} \\ &= -\frac{1}{2} \mathbf{y}^T \mathbf{y} \cdot \tau_{\text{noise}} + \mathbf{y}^T \tau_{\text{noise}} \mathbf{S} \mathbf{Q}_C^{-1} \mathbf{S} \left(\frac{\partial \tau_{\text{noise}}}{\partial \log(\tau_{\text{noise}})} \right) \mathbf{y} + \\ &\quad - \frac{1}{2} \mathbf{y}^T \tau_{\text{noise}} \mathbf{S} \mathbf{Q}_C^{-1} \left(\frac{\partial}{\partial \log(\tau_{\text{noise}})} \mathbf{Q}_C \right) \mathbf{Q}_C^{-1} \mathbf{S}^T \tau_{\text{noise}} \mathbf{y} \\ &= -\frac{1}{2} \mathbf{y}^T \mathbf{y} \cdot \tau_{\text{noise}} + \boldsymbol{\mu}_C^T \mathbf{S}^T \mathbf{y} \cdot \tau_{\text{noise}} - \frac{1}{2} \boldsymbol{\mu}_C^T \mathbf{S}^T \mathbf{S} \boldsymbol{\mu}_C \cdot \tau_{\text{noise}} \\ &= -\frac{1}{2} (\mathbf{y} - \mathbf{A} \boldsymbol{\mu}_C)^T (\mathbf{y} - \mathbf{A} \boldsymbol{\mu}_C) \cdot \tau_{\text{noise}}.\end{aligned}$$

Together these expressions give

$$\begin{aligned}\frac{\partial \log(\pi(\boldsymbol{\theta}, \tau_{\text{noise}} | \mathbf{y}))}{\partial \log(\tau_{\text{noise}})} &= \frac{\partial}{\partial \log(\tau_{\text{noise}})} \log(\pi(\boldsymbol{\theta}, \tau_{\text{noise}})) + \frac{N}{2} - \frac{1}{2} \text{Tr} [\mathbf{Q}_C^{-1} \mathbf{S}^T \mathbf{S} \cdot \tau_{\text{noise}}] + \\ &\quad - \frac{1}{2} (\mathbf{y} - \mathbf{A} \boldsymbol{\mu}_C)^T (\mathbf{y} - \mathbf{A} \boldsymbol{\mu}_C) \cdot \tau_{\text{noise}}\end{aligned}$$

C.3 Implementation

The derivative $\frac{\partial}{\partial \theta_i} \mathbf{Q}_c$ can be calculated quickly since it is a simple functions of θ . The trace of the inverse of a matrix A times the derivative of a matrix B only requires the values of the inverse of A for non-zero elements of B . In the above case the two matrices have the same type of non-zero structure, but it can happen that specific elements in the non-zero structure are zero for one of the matrices. This way of calculating the inverse only at a subset of the locations can be handled as described in Gelfand et al. (2010, Sections 12.1.7.10–12.1.7.12).

References

- Bolin, D. and F. Lindgren. 2011. *Spatial models generated by nested stochastic partial differential equations, with an application to global ozone mapping*, The Annals of Applied Statistics **5**, no. 1, 523–550.
- Damian, Doris, Paul D. Sampson, and Peter Guttorp. 2001. *Bayesian estimation of semi-parametric non-stationary spatial covariance structures*, Environmetrics **12**, no. 2, 161–178.
- Damian, Doris, Paul D. Sampson, and Peter Guttorp. 2003. *Variance modeling for nonstationary spatial processes with temporal replications*, Journal of Geophysical Research: Atmospheres **108**, no. D24, n/a–n/a.
- Diggle, P.J., P.J. Ribeiro, and P. Justiniano. 2007. *Model-based Geostatistics*, Springer New York.
- Fuentes, Montserrat. 2001. *A high frequency kriging approach for non-stationary environmental processes*, Environmetrics **12**, no. 5, 469–483.
- . 2002a. *Interpolation of nonstationary air pollution processes: a spatial spectral approach*, Statistical Modelling **2**, no. 4, 281–298, available at <http://smj.sagepub.com/content/2/4/281.full.pdf+html>.
- . 2002b. *Spectral methods for nonstationary spatial processes*, Biometrika **89**, no. 1, 197–210, available at <http://biomet.oxfordjournals.org/content/89/1/197.full.pdf+html>.
- Fuglstad, Geir-Arne, Finn Lindgren, Daniel Simpson, and Håvard Rue. 2013. *Exploring a New Class of Non-stationary Spatial Gaussian Random Fields with Varying Local Anisotropy*. Submitted.
- Gelfand, A., P.J. Diggle, P. Guttorp, and M. Fuentes. 2010. *Handbook of Spatial Statistics*, CRC Press.
- Gneiting, T., A.E. Raftery, A.H. Westveld III, and T. Goldman. 2005. *Calibrated probabilistic forecasting using ensemble model output statistics and minimum crps estimation*, Monthly Weather Review **133**, no. 5, 1098–1118.
- Haas, Timothy C. 1990a. *Kriging and automated variogram modeling within a moving window*, Atmospheric Environment. Part A. General Topics **24**, no. 7, 1759–1769.
- . 1990b. *Lognormal and moving window methods of estimating acid deposition*, Journal of the American Statistical Association **85**, no. 412, 950–963, available at <http://amstat.tandfonline.com/doi/pdf/10.1080/01621459.1990.10474966>.
- Hastings, David A., Paula K. Dunbar, Gerald M. Elphinstone, Mark Bootz, Hiroshi Murakami, Hiroshi Maruyama, Hiroshi Masaharu, Peter Holland, John Payne, Nevin A. Bryant, Thomas L. Logan, J.-P. Muller, Gunter Schreier, and John S. MacDonald. 1999. *The global land one-kilometer base elevation (globe) digital elevation model, version 1.0*, <http://www.ngdc.noaa.gov/mgg/topo/globe.html>.
- Higdon, David. 1998. *A process-convolution approach to modelling temperatures in the north atlantic ocean*, Environmental and Ecological Statistics **5**, 173–190. 10.1023/A:1009666805688.
- Ingebrigtsen, Rikke, Finn Lindgren, and Ingelin Steinsland. 2013. *Spatial Models with Explanatory Variables in the Dependence Structure of Gaussian Random Fields based on Stochastic Partial Differential Equations*. Submitted.
- Johns, Craig J, Douglas Nychka, Timothy G F Kittel, and Chris Daly. 2003. *Infilling sparse records of spatial fields*, Journal of the American Statistical Association **98**, no. 464, 796–806.
- Kim, Hyoungh-Moon, Bani K Mallick, and C. C Holmes. 2005. *Analyzing nonstationary spatial data using piece-wise gaussian processes*, Journal of the American Statistical Association **100**, no. 470, 653–668, available at <http://amstat.tandfonline.com/doi/pdf/10.1198/016214504000002014>.
- Lindgren, Finn and Håvard Rue. 2008. *On the second-order random walk model for irregular locations*, Scandinavian journal of statistics **35**, no. 4, 691–700.

- Lindgren, Finn, Håvard Rue, and Johan Lindström. 2011. *An explicit link between gaussian fields and gaussian markov random fields: the stochastic partial differential equation approach*, Journal of the Royal Statistical Society: Series B (Statistical Methodology) **73**, no. 4, 423–498.
- Paciorek, Christopher J. and Mark J. Schervish. 2006. *Spatial modelling using a new class of nonstationary covariance functions*, Environmetrics **17**, no. 5, 483–506.
- Petersen, K. B. and M. S. Pedersen. 2012. *The matrix cookbook*, Technical University of Denmark. Version 20121115.
- Rue, Håvard and Leonard Held. 2005. *Gaussian Markov random fields: Theory and applications*, Monographs on Statistics and Applied Probability, vol. 104, Chapman & Hall, London.
- Sampson, Paul D. and Peter Guttorp. 1992. *Nonparametric estimation of nonstationary spatial covariance structure*, Journal of the American Statistical Association **87**, no. 417, 108–119, available at <http://www.tandfonline.com/doi/pdf/10.1080/01621459.1992.10475181>.
- Schmidt, Alexandra M., Peter Guttorp, and Anthony O’Hagan. 2011. *Considering covariates in the covariance structure of spatial processes*, Environmetrics **22**, no. 4, 487–500.
- Schmidt, Alexandra M. and Anthony O’Hagan. 2003. *Bayesian inference for non-stationary spatial covariance structure via spatial deformations*, Journal of the Royal Statistical Society: Series B (Statistical Methodology) **65**, no. 3, 743–758.
- Whittle, P. 1954. *On stationary processes in the plane*, Biometrika **41**, no. 3/4, pp. 434–449 (English).